SOLID BODY ROTATION FLOW FOR PARTICLE IMAGE VELOCIMETRY CALIBRATION

B.A.A. Gomes, azevedo@mec.puc-rio.br
R. L. Thompson, roney@mec.puc-rio.br
L.F.A. Azevedo, lfaa@mec.puc-rio.br
Departamento de Engenharia Mecânica, Pontifícia Universidade Católica – PUC/Rio
R. Marquês de São Vicente 225- Gávea, 22453-900 Rio de Janeiro, RJ, Brasil

Abstract. *A solid body rotation flow experiment was constructed with the objective of calibrating a Particle Image Velocimetry system (PIV). The PIV system determines the velocity field based on the analysis of consecutive images of tracer particles dispersed in the fluid and illuminated externally by a pulsed laser light. In the present case the images are analyzed by a cross-correlation algorithm yielding particle displacement fields. In order to evaluate the influence of the several parameters that control the accuracy of the PIV technique, a solid body rotation flow was chosen as a simple two-dimensional flow of known velocity field. A cylindrical glass container was mounted on a rotating table of controlled angular speed. Metallic coated hollow glass spheres of mean diameter of 30 μm were used as tracers particles in water. A geometrical calibration tool was designed so as to allow the flow coordinate system to be transformed from the camera xy frame of reference to the cylindrical frame of reference of the rotating tank. An uncertainty analysis was performed on the variables that affect the calibration procedure. Excellent agreement was found between measured and predicted velocities.*

Key-words:.*Velocity measurements, Particle Image Velocimetry, Calibration*

1. INTRODUCTION

Particle Image Velocimetry has become a widely used tool for transient fluid flow measurements over extensive areas of the flow. The now established technique has been employed successfully in flows ranging from low Reynolds number to supersonic flows (Adrian, 1996). Commercial systems are already available to handle complex flow situations. An extensive literature discusses all aspects of the technique (Raffel et al.,1998). However, due to the complexity of the technique and to the elevated number of parameters that affect the results obtained with its use, it is recommended that an experimental program utilizing Particle Image Velocimetry as the measuring technique be preceded by a calibration experiment. This type of experiment will allow the user to gain confidence on this complex technique and to evaluate the relative importance of the several physical and computational parameters that affect the accuracy of the velocity measurements.

The purpose of the present paper is to report on a calibration experiment designed to be

used for testing the several parameters that control the technique, to find its limitations and, thereby, improve the confidence on its use as a research tool.

The calibration experiment chosen was the solid body rotation velocity field attained by a body of fluid when rotated around a vertical axis with constant angular speed. This type of flow was chosen for having an exact solution independent of fluid properties. Also, it is relatively easy to construct and provides a wide range of flow velocities to be tested.

2. EXPERIMENTS

Prior to describing the details of the calibration experiment constructed, a brief review of the Particle Image Velocimetry technique employed is presented. For a complete description of the technique, the interested reader is referred to the works of Adrian (1996).

2.1. The Particle Image Velocimetry Technique

Particle Image Velocimetry is an optical technique capable of performing instantaneous velocity measurements over extensive areas of the flow field. The technique is based on the analysis of consecutive images of tracer particles dispersed in the fluid and illuminated externally by a plane of light. By this method, depending on the particle concentration, several thousand velocity vectors can be measured simultaneously.

Figure 1 shows a schematic view of the velocity measurement system employed. Light from a 5-Watt laser, model Innova 70 by Coherent, is modulated by a Pockels cell, model 3455 manufactured by Connoptics. The beam exiting the Pockels cell is transformed into a diverging light sheet by a cylindrical lens. A spherical lens is also employed to control the thickness of the light sheet. The light sheet reaches the test section, after passing through the tank glass wall, illuminating the region of interest in the rotating tank. The water in the tank was seeded with 30 μm, metallic-coated, hollow glass spheres particles. The particles have density of 1.65 g/cm^3.

The images of the particles in the flow were registered by a TSI 60040 CCD cross correlation camera, mounted orthogonally to the illuminating light sheet. The camera has a spatial resolution of 640 x 480 pixels and a fixed frame rate of 30 frames per second. The camera was equipped with a 18-108 mm zoom lens. The images were digitized by a TSI model 6157 frame grabber, running on a Pentium 150 MHz computer.

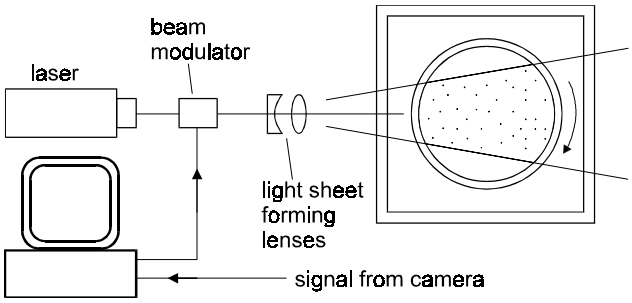

Figure 1 – Schematic view of the velocity measurement optical setup.

The synchronization of the camera with the laser modulation by the Pockels cell and the frame grabber was performed by a TSI model 60030 synchronizer. The synchronizer locked to the start-of-frame camera signal and waited for a preset time delay to activate the Pockels cell, producing the first illuminating pulse. After a specified time interval, the synchronizer triggered the Pockels cell again, producing the second illuminating pulse. In this way, the first light pulse was registered in one camera frame, while the second one was registered in the subsequent frame, with a time interval different from the fixed 33 ms interval characteristic of the camera. This technique, known as frame straddling, allows that images with relatively small time intervals be registered using cameras with standard frame rates. For instance, in

the case of the camera used in the present experiments, intervals between images as low as 30 μs can be registered in a 30 frames per second camera.

The duration of each light pulse and the time between pulses can be set in the synchronizer. The time between pulses is the single most important parameter that determines the success of the measuring technique, and depends on the magnitude of the flow velocity being measured. Faster flows require smaller times between pulses to guarantee that the images of the particles registered in the second frame have not displaced too far from their positions in the first frame. If this is not the case, the correlation between the two images will fail to produce the desired particle displacements.

The larger the duration of the illuminating pulse, the brighter is the particle images and the easier is to register them in the camera. The duration of the pulses is limited by the particle velocity. Faster particles require small pulse duration, to avoid particle streaking.

Image Analysis. The velocity field was determined by cross correlating the two images of the particles corresponding to the two consecutive light pulses. Cross correlation is a very effective and robust technique of analyzing images with high density of particles, yielding particle displacement fields without directional ambiguity. A brief description of the cross correlation method is presented next. Further details of cross correlation as applied to PIV images can be found in several references (e.g., Adrian, 1996 and Almeida, 1997).

Figures 2(a) and (b) represent typical particle images captured at two consecutive time instants, t (image 1) and t + Δt (image 2). A window is selected in image 1 containing, at its center, the point where the velocity will be determined. The dimensions of this window, called the base window, are such that a reasonable number of particle images is contained in the window area. Typically, 10-20 particles produce good results (Adrian, 1996). If the window area is sufficiently small that velocity gradients are not strong, it is highly probable that the same pattern of particles in window 1 will be found somewhere in image 2. To find the location of the pattern of window 1 in image 2, a new window is selected in image 2. This window, the search window, is centered at the same coordinates of the point of measurement, but in image 2, and is used to limit the search area in image 2.

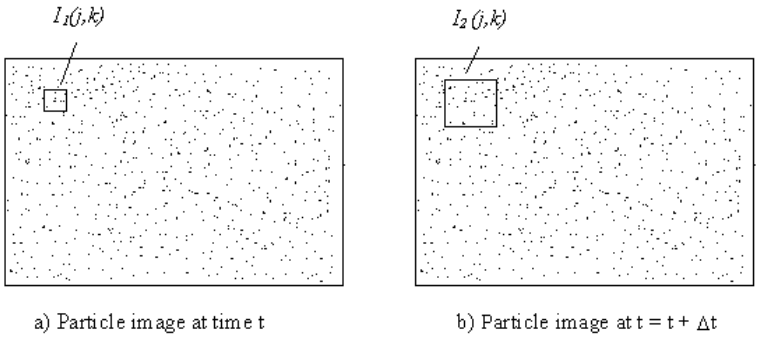

Figure 2 – Typical high particle concentration images.

In Fig. 3, $I_1(j,k)$ and $I_2(j,k)$ are the two windows, and (j,k) are indexes of the JxK pixels base window, positioned in the MxN pixels search window. The coordinates of the point where the measurement is being performed are $(x_1 y_1)$.

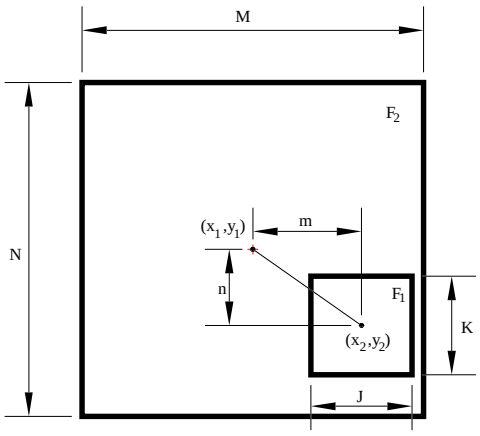

Figure 3 – The base and search windows for cross correlation analysis of the particle images.

By cross correlating the two windows, the pattern of window 1 is overlaid on window 2, with a pixel offset corresponding to the displacement being checked. The cross correlation

function is the sum of the products of the aligned pixel values, and is given, in a normalized form, as (Almeida, 1997),

$$R(m,n) = \frac{\sum_j \sum_k I_1(j,k)\, I_2(j-m,k-n)}{\left\{\left[\sum_j \sum_k I_1^2(j,k)\right]\left[\sum_j \sum_k I_2^2(j-m,k-n)\right]\right\}^{1/2}} \tag{1}$$

The position in window 2 where the correlation function R displays its largest value has coordinates (x_2,y_2), and determines the location where window 1 is found in window 2. The velocity vector is given by

$$u = (x_2\text{-}x_1)/M\,\Delta t \quad \text{and} \quad v = (y_2\text{-}y_1)/M\,\Delta t \tag{2}$$

where, M is the magnification of the image and Δt the time interval between the two images.

Since the correlation function is normalized, its values vary between zero and one. However, due to deformations imposed on the pattern of window 1 by the flow, or by the possibility of particles being lost out of window 2, the correlation value will be smaller than one. For this reason, it is necessary to impose a threshold value bellow which the correlation is not considered valid.

A typical map of the correlation function is presented in Fig. 4. The coordinates of the base region are (x_1=0, y_1=0), and the coordinates (x_2,y_2) correspond to the point where the correlation is maximum, that is, the tallest peak in the correlation map.

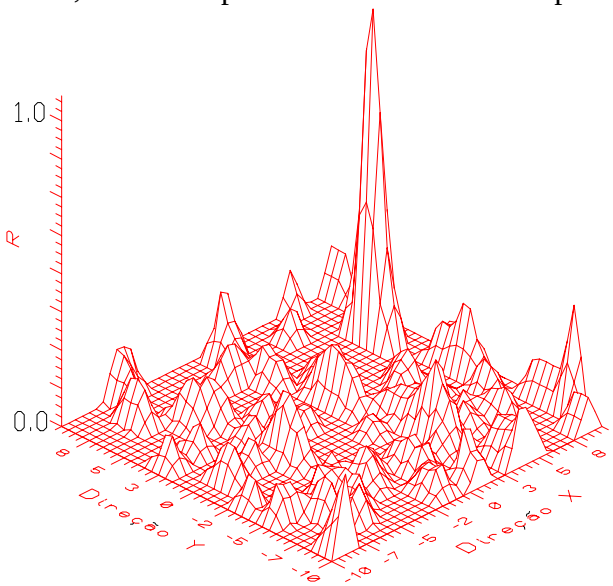

Figure 4 – Typical map of cross correlation function.

The calculation of the cross correlation function by the convolution of the two image functions as presented in the previous paragraphs, is a computationally intensive task. A more efficient alternative is to compute the cross correlation function using two dimensional Fast Fourier Transforms (FFT). In this method, the FFT of window 1 is multiplied by the complex conjugate of the FFT of window 2. The inverse FFT of the multiplication result is the correlation function. The results to be presented in this paper were obtained using this method, as implemented in the INSIGHT Particle Image Velocimetry software by TSI.

2.2.Calibration Test Section

The test section employed in the calibration experiments is shown schematically in Fig. 5 The heart of the test section was a cylindrical glass tank with height of 350 mm and internal diameter of 178 mm. A cylindrical cover was specially designed to seal the water with the tracer particles in the tank and to allow visual access for the camera to the illuminated plane. To this end, a glass window was fitted into a circular plexiglass frame. This frame housed an O-ring that contacted the external surface of the tank providing the desired sealing.

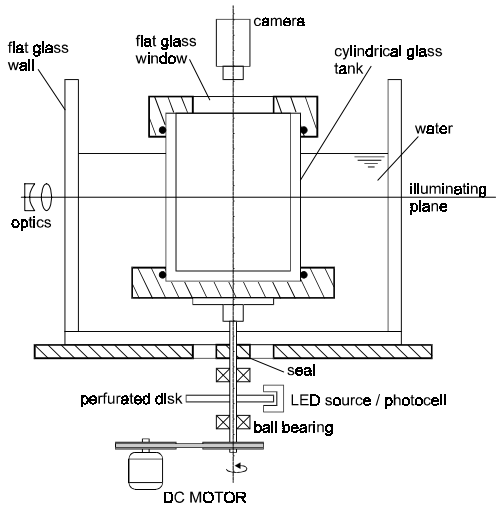

Figure 5 – Test section for velocity measurements

The tank was rotated by variable speed DC motor and pulley assembly. The angular speeds attained by this driving unit ranged from 40 to 250 RPM. The driving shaft was supported by two ball bearings and connected to a specially machined plexiglass driving flange. This flange was designed to receive the glass tank. An O-ring housed in the plexiglass flange provided a tight fit to the tank, which guaranteed that the tank would be driven by the motor without slipping. The driving shaft passed through the bottom of an open-topped, square tank, which surrounded the cylindrical tank. This square tank was assembled from four 6-mm-thick, 400x400-mm, vertical glass walls and a 12-mm-thick plexiglass bottom plate. A spring-loaded ceramic seal provided the sealing for the shaft passing through the bottom plate. The space between the square tank and the cylindrical tank was filled with water so as to minimize the refraction and reflection of the illuminating laser sheet passing through the curved wall of the cylindrical tank.

A 100-mm aluminum disk was mounted on the driving shaft in order to measure the tank angular speed. This disk had ten 6-mm holes drilled, equally spaced, along a circunference. The disk passed between a light source and photo sensor in such a way that the holes interrupted the light beam reaching the photo sensor. Therefore, each turn of the shaft produced ten pulses detected by a digital oscilloscope connected to the voltage output of the photo sensor. The frequency of the square wave captured by scope was used to measure the tank angular speed. Preliminary tests conducted with tank-motor assembly showed that the angular speed could me measured and maintained to within ± 1%.

Camera calibration disk. As will be described shortly in the Experimental Procedure section, the comparison of the velocity field measured by the PIV system and velocity field calculated by the angular velocity of the rotating tank, requires the knowledge of the radial position of each point selected for comparison. The velocity field obtained by the PIV system is, however, referenced to the camera Cartesian coordinate system. The calibration disk presented in Fig. 6 was constructed to allow the determination of the radial coordinate of selected points originally measured in the frame of reference of the camera.

The calibration disk was a 160-mm-diameter, 12-mm-thick plexiglass disk connected to a base disk by a shaft and a tube. The shaft could slide in the tube, so as to allow the adjustment of the height of the calibration disk. On the top surface of the top disk, a grid formed by the intersection of radial and circunferential lines was marked. These lines were accurately marked employing the dividing head of a milling machine. The grid was formed by several concentric circles, with diameters progressively increasing by 5 mm. The radial lines were marked 2 degrees apart from each other. The base disk was machined so as to perfectly fit

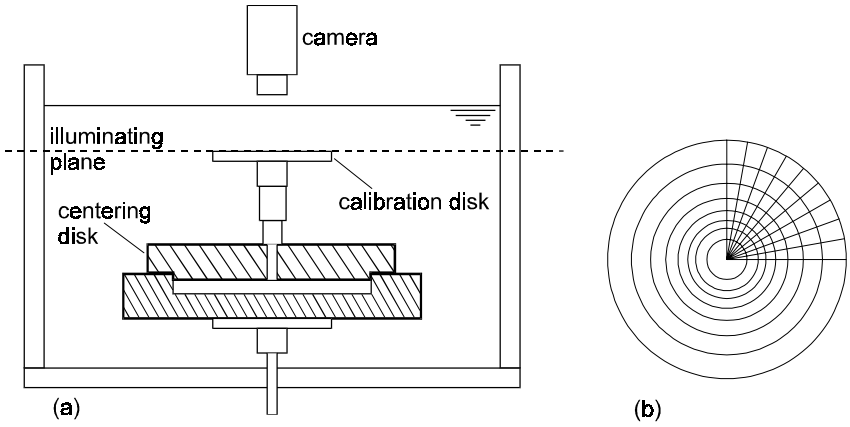

Figure 6 – Test section for camera calibration: a) side view b) topview of calibration disk

into the flange that hold the cylindrical glass tank (with the tank removed). This accurate fit guaranteed that the center of rotation of the tank coincided with the center of the camera calibration disk

2.3.Experimental Procedure

The experimental procedure employed involved the velocity measurement experiments and the camera calibration experiments.

For the velocity measurements, the cylindrical glass tank was filled with distilled water containing the tracer particles. The top cover of the tank was mounted in place and the air trapped during the filling operation was purged through the vent hole. The tank was then mounted into the plexiglass driving frame. The square glass tank was filled with water. The laser was turned on, and the camera focused on the particles in the illuminating plane. The camera was then firmly secured in place by locking bolts. The angular speed for the particular experiment was set at the DC motor controller. The time necessary for attaining solid body rotation in the tank was known from test runs conducted previously. After this time, a series of pairs of images of the flow was recorded and latter processed. The time interval between each image pair set in the synchronizer dependeds on the angular speed being studied and was determined from test runs.

After the flow images corresponding to all the angular speeds of interest were recorded, the camera calibration experiments were initiated. Firstly, the square tank was emptied and the cylindrical tank removed from the driving plexiglass frame. The base disk supporting the camera calibration disk was mounted in the driving plexiglass frame. The height of the camera calibration disk was carefully adjusted so that its top surface was touched by the laser illuminating plane. With this procedure, it was assured that the camera calibrating disk was at the same vertical position as the tracer particles previously recorded. The square glass tank was then filled with water, up to the same level as that employed in the velocity measurement experiments. An image of the grid marked on the top face of the calibration disk was captured. Two points on the grid were marked and their coordinates in the image frame of reference recorded in pixel units. These two points, with known radial and circunferential, coordinates were used to establish the relationship between the camera Cartesian frame of reference and the polar frame of reference centered on the axis of rotation of the tank. This procedure allowed the comparison of the velocity vectors measured by the PIV technique with those predicted for the solid body rotation flow.

As a final calibration procedure, a scale was positioned on the top surface of the camera calibration disk. Two images of the scale were captured: one with the scale aligned along the

horizontal axis of the camera frame, and one with the scale aligned with the vertical axis of the camera. These two images were used to determine the horizontal and vertical scale factors for the camera, i.e, to transform the velocity measurements from pixels/second to meters/second units.

2.4.Coordinate System Transformation

The procedure employed to determine the radial coordinate of the points where velocity measurements were performed is now outlined. Figure 7 was prepared to facilitate the description of the geometric transformation equations employed. In this figure, the camera field of view is represented as a rectangle within the circular area of the flow field.

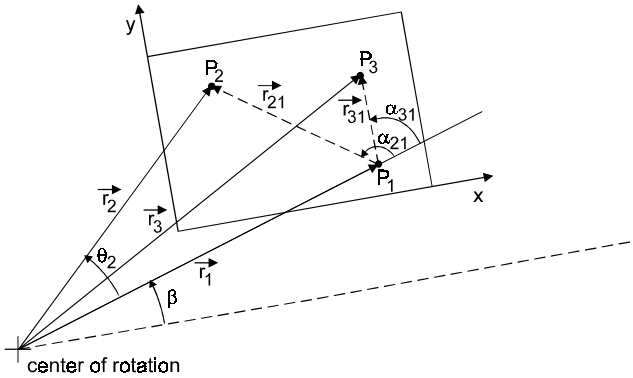

Figure 7 – Camera and tank frames of reference

Point P_1 and P_2 are the calibration points that had its radial and circunferential coordinates (r_1, θ_1 and r_2, θ_2) measured with the aid of the calibration disk, as described in the previous section. The Cartesian coordinates of these points (x_1,y_1 and x_2,y_2) were measured in pixel coordinates from the calibration image captured and transformed to actual lengths by use of the horizontal and vertical scale factors, f_h and f_v. The following geometrical relations can be obtained from the figure:

$$r_2 \cos \theta_2 = r_1 + r_{21} \cos \alpha_{21} \tag{3}$$

$$r_2 \sin \theta_2 = r_{21} \sin \alpha_{21} \tag{4}$$

$$r_{21} \cos \alpha_{21} = (x_2 - x_1) \cos \beta + (y_2 - y_1) \sin \beta \tag{5}$$

The solution of the above equations determines β, α_{21} and r_{21}. The knowledge of these quantities allow the determination of the radial coordinate of any point P_3 of known Cartesian coordinates (x_3,y_3). To this end, α_{31} is determined from

$$r_{31} \cos \alpha_{31} = (x_3 - x_1) \cos \beta + (y_3 - y_1) \sin \beta \tag{6}$$

and the radial position r_3 determined from the following relation valid for the triangle formed by r_1, r_3 and r_{31}.

$$r_3^2 = r_1^2 + 2\, r_1\, r_3 \cos \alpha_{31} + r_{31}^2 \tag{7}$$

2.4 Uncertainty Analysis

An uncertainty analysis was performed to estimate the level of uncertainty on the tangential velocity calculated by the solid body rotation expression $V = \omega r$. As already mentioned, the angular speed was measured by the perforated disk and a photo sensor. The radial position of a point of interest was determined by its pixel coordinates in the camera frame of reference, followed by a geometrical transformation to convert its coordinates to polar coordinates, using a camera calibration procedure.

The uncertainty on the velocity can be estimated by,

$$(\delta V_3/V_3)^2 = (\delta\omega/\omega)^2 + (\delta r_3/r_3)^2 \tag{8}$$

The uncertainty on the angular speed was estimated by test runs to be ±1%. The estimate of the uncertainty on R_3 requires a more elaborate procedure. The radial coordinate is a function of several parameters,

$$r_3 = g(r_1, \theta_2, r_2, x_1, y_1, x_2, y_2, x_3, y_3, f_h, f_v) \tag{9}$$

Using the procedure suggested by Moffat(1986), the uncertainty in r_3 can be evaluated by

$$(\delta r_3)^2 = [(\partial r_3/\partial z_i)(\delta z_i)]^2 \tag{10}$$

where z_i represent the variables on which the radius depend on, and δz_i the uncertainties on these variables. In the present case the partial derivatives were calculated numerically employing a program developed to calculate the geometrical transformations already described. The values for the uncertainties employed in the calculations were: $\delta r_1 = \delta r_2 = 0.1$ *mm*, $\delta\theta_2 = 0.25^o$, $\delta x_i = \delta yi = 1$ pixel, $\delta f_h = \delta f_v = 0.3$ μm/pixel. Based on these calculations, the uncertainty level on R_3 was estimated to be ±0.5%. This value combined with the uncertainty on the angular speed, gives an estimate for the uncertainty on the velocity of ±1.1%.

3. RESULTS

The comparison of velocity values measured with the PIV technique and those analytically predicted for the solid body rotation flow are presented in this section.

In order to give an overall view of the velocity field measured, Fig. 8 presents a superposition of the measured vector field and the first image of the particles that generated the velocity data. This image corresponds to a 41 x 31 mm area in the 178-mm-diameter tank. Approximately 1200 velocity vectors were determined in this flow area. However, only a few of these vectors are presented in Fig. 8 so as not to overcrowd the figure.

The comparisons between measured and predicted velocity values were performed over a single horizontal line in the camera frame of reference.

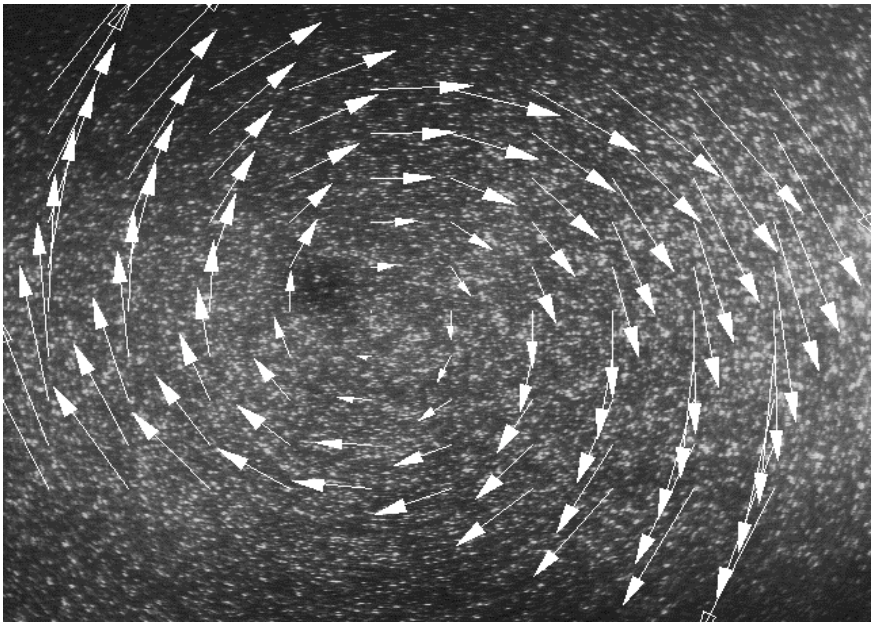

Figure 8 – Particle image and velocity field for ω = 105 RPM

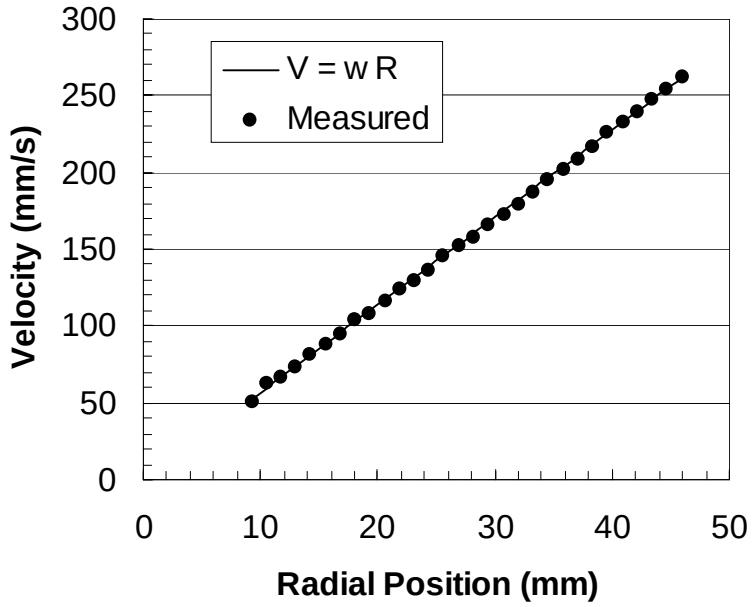

Figure 9 – Measured and predicted velocity distribution for ω = 55 RPM.

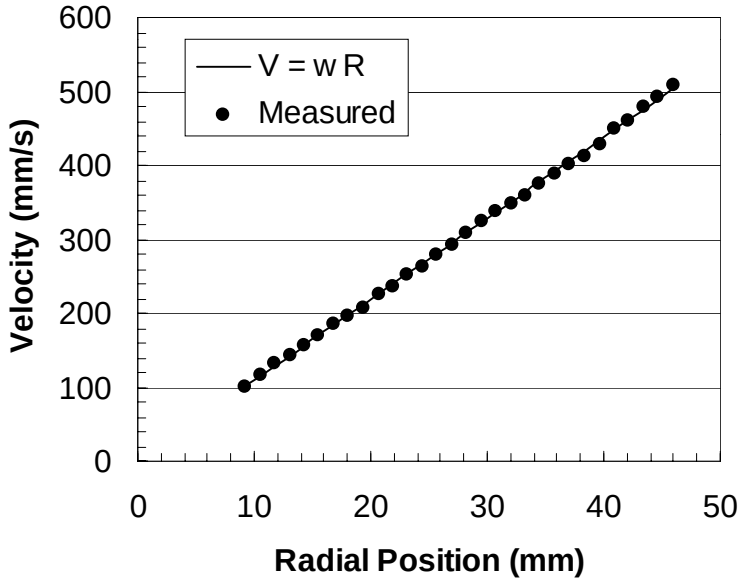

Figure 10 – Measured and predicted velocity distribution for ω = 105 RPM.

Figures 9,10 and 11 present the comparisons between measured and predicted velocity vectors for angular speeds of, respectively, 55, 105 and 222 RPM. A general observation of Figs 9-11 demonstrates the excellent agreement between measured values and those predicted for the solid body rotation flow. Indeed, for the whole velocity range investigated, the average deviations are of the order of 1%. The maximum deviations observed were of the order of 4% for the point located closest to the center of rotation. These deviations are within the uncertainty levels expected for the experiment constructed, ±1.1%., and are in agreement with the levels of uncertainty reported in the literature for PIV measurements (Adrian, 1996). It should be mentioned that these low values for the velocity uncertainty were obtained by averaging the velocity results of five consecutive measurements for each angular speed. The

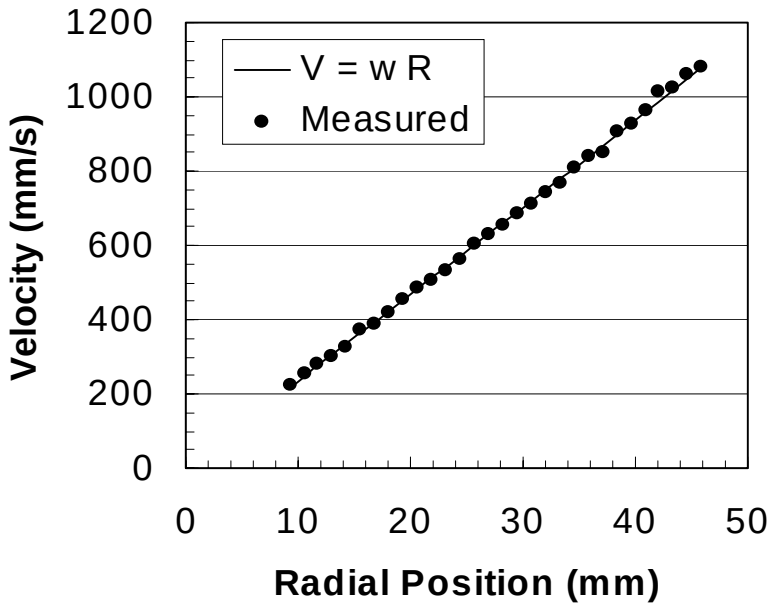

Figure 11 – Measured and predicted velocity distribution for ω = 222 RPM.

uncertainty levels for each individual measurement were typically of the order of 3%. This difference can be attributed to random fluctuations of the angular speeds of the rotating tank.

3. CONCLUSIONS

A solid body rotation flow experiment was developed with the objective of calibrating a Particle Image Velocimetry system. Consecutive images of tracer particles illuminated externally by a pulsed laser light sheet and captured by a digital camera were cross-correlated in order to yield the particle displacement field. The experiments studied tangential velocities within the range of 50 mm/s to 1 m/s. Water was the working fluid and the tracer particles were 30 μm metallic coated, hollow glass spheres.

Excellent comparison of measured and predicted results was obtained. Average deviations from the tangential speeds predicted for the solid body rotation flow were within 1%.

The results obtained attest to the quality of the Particle Image Velocimetry technique employed and encourage its use as a measuring tool for fluid flow experiments.

4. REFERENCES

Adrian, R.J., 1996, Laser Velocimetry, in Fluid Mechanics Measurements, ed. Goldstein, Taylor and Francis, Washington.

Almeida, J.A., 1997, Particle Image Velocimetry System, Doctoral Thesis, Department of Mechanical Engineering, PUC-RIO.

Moffat, R.J., 1982, Contributions to the Theory of Single-sample Uncertainty Analysis, ASME Joural of Fluids Engineering, vol. 104, pp. 250-260.

Raffel, Willert,C. and Kompenhans, J, 1998, Particle Image Velocimetry, Springer –Verlag, Berlin.